



Short communication

Electrochemical performance of Si–CeMg₁₂ composites as anode materials for Li-ion batteriesZ.W. Lu^{a,b}, G. Wang^a, X.P. Gao^{a,*}, X.J. Liu^b, J.Q. Wang^b^a Institute of New Energy Material Chemistry, Nankai University, Tianjin 300071, China^b Tianjin Institute of Power Sources, Tianjin 300381, China

ARTICLE INFO

Article history:

Received 1 June 2008

Received in revised form 11 July 2008

Accepted 16 July 2008

Available online 31 July 2008

Keywords:

Si

CeMg₁₂ alloy

Composites

Anode materials

Li-ion batteries

ABSTRACT

The Si–CeMg₁₂ composites with 30 wt.%, 40 wt.% and 50 wt.% Si, were synthesized by directly ball milling Si and CeMg₁₂ alloy. The microstructure of the Si–CeMg₁₂ composites is confirmed by X-ray diffraction (XRD) and transmission electron microscopy (TEM), respectively. It is demonstrated from TEM images that active Si nanoparticles are distributed in the inactive CeMg₁₂ matrix. The electrochemical performance of the Si–CeMg₁₂ composites as a function of Si content is investigated. The maximum reversible (charge) capacities of the ball-milled Si–CeMg₁₂ composites with 30 wt.%, 40 wt.% and 50 wt.% Si reach 470, 690 and 1080 mAh g⁻¹, respectively, after full activations. It is found that the Si–CeMg₁₂ composite with 40 wt.% Si delivers a larger reversible capacity and better cycle ability because the uniform distribution of active Si nanoparticles embedded in the CeMg₁₂ matrix, which can accommodate the volume expansion of the composite during Li-alloying/dealloying processes. After subsequent cycles, the recrystallization of Si with lattice shrinkage is observed, which is unfavorable to the Li-alloying/dealloying reaction. The degeneration of CeMg₁₂–Si composites during repeated cycling is attributed not only to the Si pulverization led by the volume change, but partially also to the irreversible phase transformation of Si.

© 2008 Elsevier B.V. All rights reserved.

1. Introduction

Si is one of the most promising anode materials for Li-ion secondary batteries because of its high theoretical capacity (Li_{4.4}Si, 4200 mAh g⁻¹), superior to the commonly used graphite (LiC₆, 372 mAh g⁻¹) [1,2]. However, the commercialization of the Si-based materials in Li-ion batteries is limited due to the poor electrochemical cycle performance, caused by a large volume change of Si particles during electrochemical alloying and dealloying processes. Nowadays, considerable effort has been made to overcome this limitation by synthesizing Si-based composites. The Si–C composites [3–6] and Si–silicides composites [7–9] are investigated because of the excellent ductility and small volume changes of carbon or silicides materials during the electrochemical cycling. Furthermore, much attention has been paid on the Si-based composites consisting of active Si and inactive metal or alloy materials with a high conductivity as a matrix, including Si–M (M = Fe, Co, Ni, Cu and Ag) [10–18], Si–TiB₂ [19], Si–SnSb [20] and Si–AB₅ [21]. Mg₂Si intermetallic compounds were reported to exhibit a large capacity and a flat potential profile [22–24]. However, the rapid degrada-

tion of the electrode was attributed to the large volume change by lithium insertion in the octahedral site of Mg₂Si [22]. It was demonstrated that Mg–Ni alloys and Mg–C composites [25,26], prepared by high energy ball-milling, had a higher electrochemical capacity for lithium insertion/extraction. Actually, rare earth–Mg alloys are more beneficial to prepare composites by high energy ball-milling, such as CeMg₁₂–Ni and Nd–Mg–Ni composites for electrochemical hydrogen storage [27,28].

In this work, the Si–CeMg₁₂ composites are synthesized by directly ball milling CeMg₁₂ and Si powder. The electrochemical performance of the resulting Si–CeMg₁₂ composites with Si nanoparticles distributed uniformly on the CeMg₁₂ matrix was evaluated by the galvanostatic method and cyclic voltammetry.

2. Experimental

The CeMg₁₂ alloy was synthesized through a salt-cover-melting process by melting the stoichiometric mixture of metallic Ce and Mg [27], and then the ingot was pulverized to 200 meshes. The Si–CeMg₁₂ composite was synthesized by directly ball milling CeMg₁₂ and Si powders (~200 nm). The Si weight percentage in Si–CeMg₁₂ composites was 30 wt.%, 40 wt.%, and 50 wt.%, respectively. The ball-milling process was performed in cyclohexane with a weight ratio of ball to powders of 20:1 at 290 rpm for 3–5 h under

* Corresponding author. Tel.: +86 22 23500876; fax: +86 22 23500876.
E-mail address: xpgao@nankai.edu.cn (X.P. Gao).

Ar atmosphere in a planetary-type ball-mill. The microstructure of the alloy powders was analyzed by X-ray diffraction (XRD, Rigaku D/max-2500) and transmission electron microscopy (TEM, FEI Tecnai 20).

The working electrodes were prepared by mixing ball-milled Si–CeMg₁₂ powders, acetylene black and polytetrafluoroethylene at the weigh ratio of 10:3:2.25 into paste, then by roll pressing the paste into an electrode film, and finally by pressing the film onto a Cu film. Metal lithium was used as the counter and reference electrode. The electrolyte was 1 M LiPF₆ in a mixture of ethylene carbonate (EC), propylene carbonate (PC), and dimethyl carbonate (DMC). The volume ratio of EC:PC:DMC in the mixture was 6:3:1. The cells were assembled in an atmosphere of high-purity argon in a glove box. Discharge–charge measurements of the cells were carried out at the current density of 100 mA g^{−1} between the potential range of 0.02–1.2 V (vs Li⁺/Li) using a LAND-CT2001A instrument. Cyclic voltammograms (CVs) and electrochemical impedance spectra (EIS) were taken using an IM6e electrochemical workstation at 25 °C.

3. Results and discussion

XRD patterns of ball-milled Si–CeMg₁₂ composites with 30 wt.%, 40 wt.% and 50 wt.% Si are shown in Fig. 1. The strong diffraction peaks of Si and the weak diffraction peaks of the CeMg₁₂ appear for all ball-milled Si–CeMg₁₂ composites. The crystalline Si has a face-centered cubic structure with a lattice parameter of $a = 5.430 \text{ \AA}$ (*Fd* $\bar{3}m$ (2 2 7), JCPDS 89-2955). There are no traces of Mg–Si alloy or other metal silicides formed during the ball-milling process, which serve as active material of electrochemical Li-alloying reaction in previous reports [22,23]. It means that the interaction between Si and CeMg₁₂ during the ball milling process is weak, and CeMg₁₂ alloy may act only as the inactive matrix to support active Si particles in the Si–CeMg₁₂ composites.

TEM images of ball-milled Si–CeMg₁₂ composites are illustrated Fig. 2. In most cases, Si particles with a size of 50–80 nm are dispersed on the CeMg₁₂ alloy matrix according to mass-thickness contrast. Especially in the Si–CeMg₁₂ composite with 40 wt.% Si, Si nanoparticles are uniformly inlaid on the alloy matrix (Fig. 2b). The supported distribution can prevent Si nanoparticles from aggregating and insure the good cycle stability of the composites as anode materials for lithium ion batteries. In the composite with 50 wt.% Si, a few of large Si particles of over 200 nm coexist with small Si

particles on the alloy matrix (Fig. 2c). The calculated interference fringe spacing of Si from the intensity line profile for a selected area of the Si grain as inserted in Fig. 2d is about 0.34 nm, which is close to the interplanar distance of (1 1 1) planes of Si. It means that nanocrystalline Si exists in ball-milled Si–CeMg₁₂ composites, in agreement with XRD patterns.

The cycle life of ball-milled Si–CeMg₁₂ composites at the current density of 100 mA g^{−1} is presented in Fig. 3. In the case of the ball-milled CeMg₁₂ alloy, a low reversible electrochemical capacity of 57 mAh g^{−1} is obtained, indicating the electrochemical inactivity of the ball-milled CeMg₁₂ alloy for Li-alloying/dealloying reaction due to the strong interaction between Ce and Mg atoms in CeMg₁₂ alloy. The electrochemical capacities of ball-milled Si–CeMg₁₂ composites increase with the addition of the enhanced Si content into CeMg₁₂ alloy. Obviously, there is an activation process in the electrochemical Li-alloying/dealloying reaction of all the composites, and the electrochemical capacities gradually increase within 10 cycles (depended on the Si content). The maximum reversible (charge) capacities of the ball-milled Si–CeMg₁₂ composites with 30 wt.%, 40 wt.% and 50 wt.% Si can reach 470, 690 and 1080 mAh g^{−1}, respectively, after full activations. Compared with the rapid decay of the Si–CeMg₁₂ composite with 50 wt.% Si, the cycle stability of the composite with 40 wt.% Si is better. The reversible (charge) electrochemical capacity of 550 mAh g^{−1} is obtained for the composite with 40 wt.% Si after 30 cycles. Usually, the cycle stability of Si-based composites is mostly related to material microstructure and highly depended on Si content [29]. The improvement of the cycle stability of the Si–CeMg₁₂ composite with 40 wt.% Si is mainly attributed to a uniform distribution of active Si nanoparticles embedded in the CeMg₁₂ matrix as shown in TEM, which can accommodate the volume expansion of the composite during Li-alloying/dealloying processes. In comparison, it seems that the capacity fade is still unsatisfied for the sample with 30 wt.% Si, although more inactive CeMg₁₂ material is involved in the sample. It means that the uniform distribution of active Si nanoparticles in the CeMg₁₂ matrix is more important for the cycle stability of the Si–CeMg₁₂ composite.

Typically, the discharge and charge profile of the ball-milled Si–CeMg₁₂ composite with 40 wt.% Si at the current density of 100 mA g^{−1} is indicated in Fig. 4. It is found that the potential curve of the first discharge process is obviously different from the third one. The high discharge potential is found at 0.6–0.8 V (vs Li⁺/Li), which is mainly attributed to the formation of a solid electrolyte interface (SEI) film on the surface of the electrode with acetylene black [15,30]. In the subsequent cycles, the discharge (Li-alloying) process of the composites is conducted around 0.2 V, suggesting the irreversible phase transformation of silicon from crystalline to amorphous state by electrochemically driven solid-state amorphization [29,31,32].

In order to confirm the mechanism of the electrochemical alloying/dealloying reaction of ball-milled Si–CeMg₁₂ composites, cyclic voltammograms (CVs) were measured as shown in Fig. 5. One cathodic peak near 0.5 V in the first cycle is related to the high discharge potential in Fig. 4, which disappears in the following cycles. Two anodic peaks, located at 0.37 and 0.64 V, respectively, gradually evolve from the first cycle, and become clearer after the following cycles. Moreover, the activation processes are also found in the CV curves, and the peak area of the anodic Li-dealloying process located at around 0.6–0.7 V increases gradually, in agreement with the change in charge–discharge curves. In the anodic process, the two oxidation peaks, located at around 0.4 V and 0.8 V, are related to two electrochemical Li-dealloying processes of the Si–CeMg₁₂ composites. The appearance of two Li-dealloying peaks can be attributed to the alloying/dealloying process of Li_xSi alloys with different compositions [21,29].

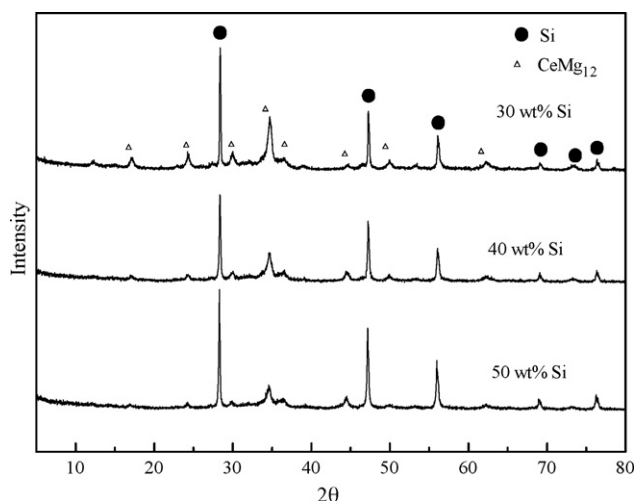


Fig. 1. XRD patterns of ball-milled Si–CeMg₁₂ composites.

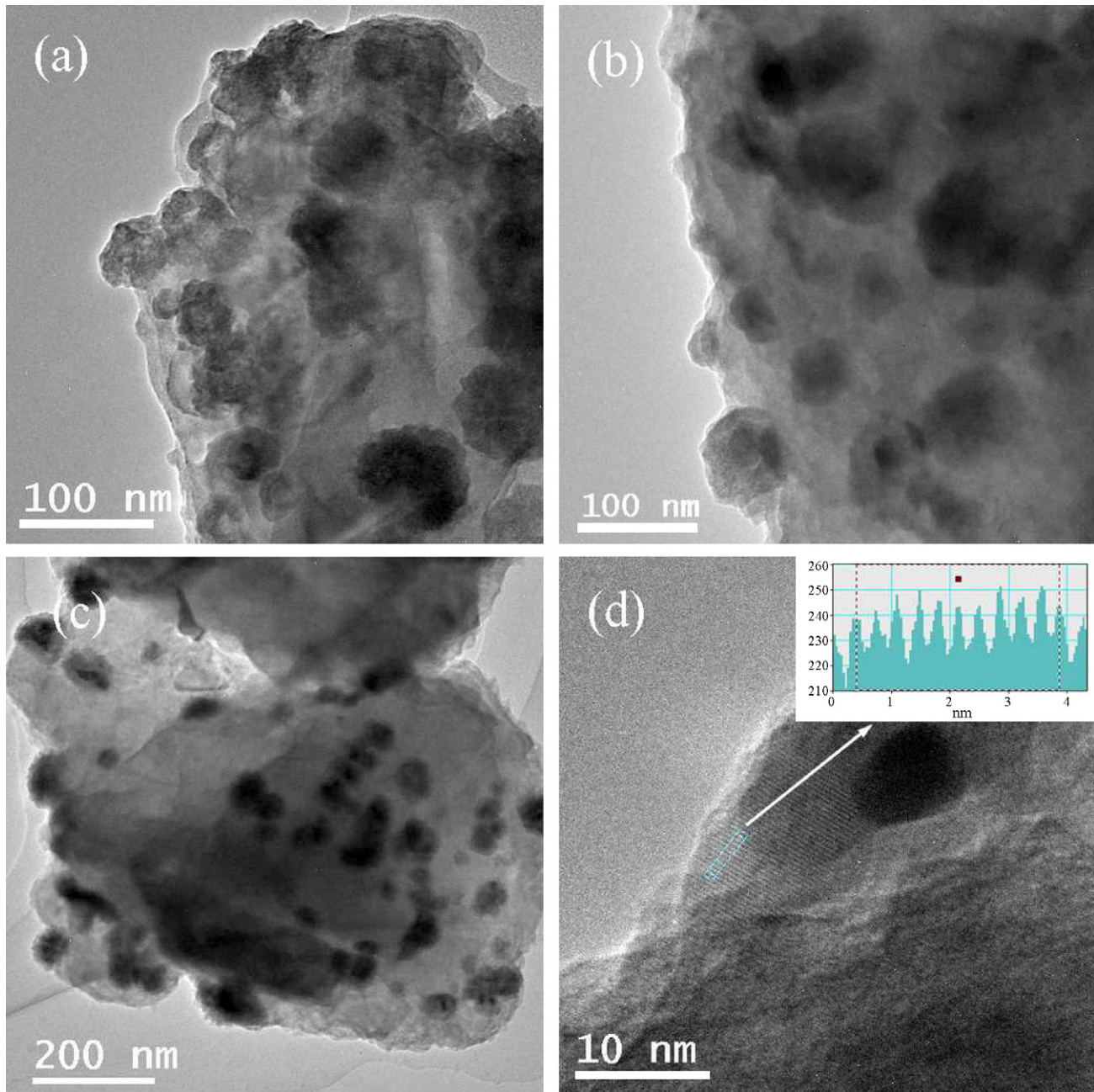


Fig. 2. TEM and HRTEM images of ball-milled Si–CeMg₁₂ composite with: 30 wt.% Si (a), 40 wt.% Si (b), and 50 wt.% Si (c). HRTEM image of the Si–CeMg₁₂ composite containing with 40 wt.% Si is indicated in (d) and the intensity line profile of nanocrystalline Si is inserted in (d).

XRD patterns of the Si–CeMg₁₂ composite with 40 wt.% Si at charged state after different cycles are shown in Fig. 6. The diffraction peaks of Si nanoparticles disappear gradually with increasing cycles. In the meanwhile, a trace of crystalline Li–Si alloys can be detected in the XRD patterns at fully discharged states after 2nd cycle. The diffraction intensity of crystalline Li–Si alloys decreases gradually during further cycling owing to the formation of amorphous Li–Si alloys and Si during the electrochemical Li-alloying/dealloying process [31,32]. In addition, the CeMg₁₂ alloy still remains the inherent structure as the inactive matrix with increasing cycles. However, a diffraction peak at 40.18° is detected at fully charged and discharged states after subsequent cycles, which can be indexed as Si with a face-centered cubic structure (*Fm*3*m* (2 2 5), JCPDS 35-1158). Although the Si has the same face-

centered cubic structure after the recrystallization during repeated cycling, but the lattice parameter of newly formed Si ($a = 3.903 \text{ \AA}$) is smaller than that of the original Si ($a = 5.430 \text{ \AA}$). The formation of shrunken Si is probably due to the electrochemically driven phase transformation and recrystallization as schemed in Fig. 7, accompanying the nucleation and growth of amorphous silicon during repeated lithium insertion/extraction cycling [31]. Therefore, the Si structure transition, including amorphization and recrystallization process of Si, is involved in the Si–CeMg₁₂ composites during Li-alloying/dealloying reactions. Undoubtedly, the lattice shrinking of Si is unfavorable to the Li-alloying/dealloying reaction. The degeneration of CeMg₁₂–Si composites during repeated cycling, is not only attributed to the Si pulverization led by volume change, but also partly due to the irreversible phase transformation of Si.

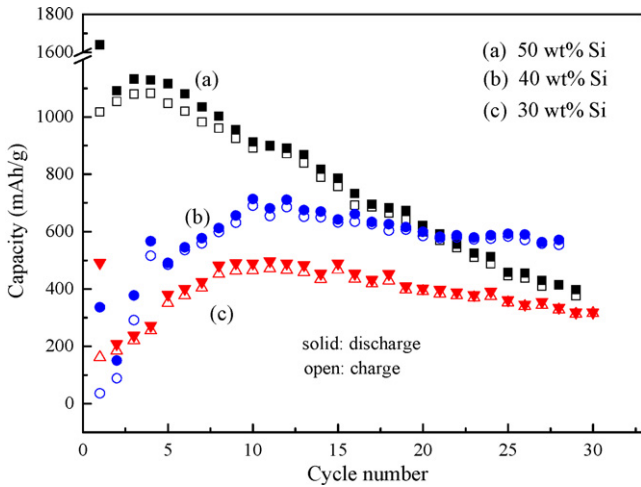


Fig. 3. The cycle life of ball-milled Si-CeMg₁₂ composites.

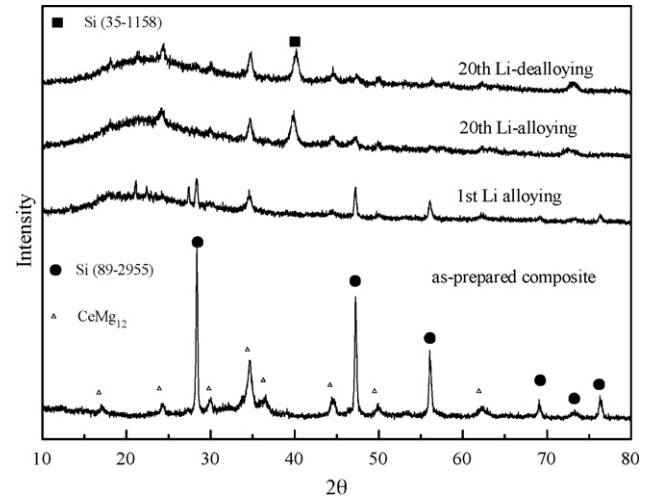


Fig. 6. XRD patterns of the ball-milled Si-CeMg₁₂ composite with 40 wt.% Si at discharged state after different cycles.

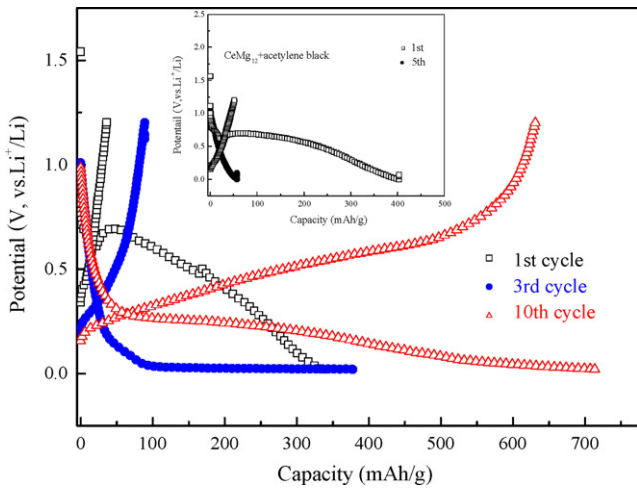


Fig. 4. Charge and discharge profiles of the ball-milled Si-CeMg₁₂ composite with 40 wt.% Si. Charge and discharge profiles of CeMg₁₂-acetylene black are inserted.

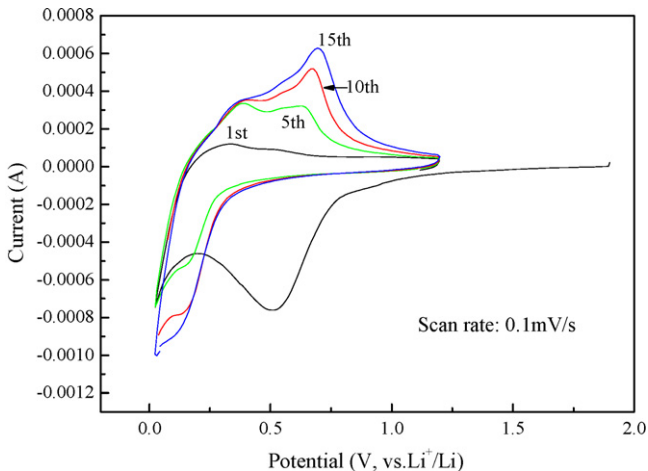


Fig. 5. Cyclic voltammograms of the ball-milled Si-CeMg₁₂ composite with 40 wt.% Si.

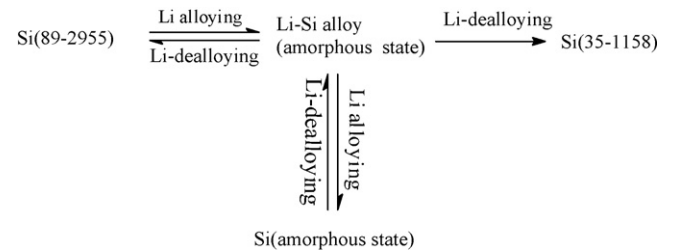


Fig. 7. The scheme for Si structure transitions in Si-CeMg₁₂ composite during electrochemical cycling.

4. Conclusions

In this work, the Si-CeMg₁₂ composites with 30 wt.%, 40 wt.% and 50 wt.% Si, were synthesized by directly ball milling Si and CeMg₁₂ alloy. The CeMg₁₂ alloy still remains the inherent structure as the inactive matrix with increasing cycles. The maximum reversible (charge) capacities of the ball-milled Si-CeMg₁₂ composites with 30 wt.%, 40 wt.% and 50 wt.% Si can reach 470, 690 and 1080 mAh g⁻¹, respectively, after full activations. The reversible (charge) electrochemical capacity of 550 mAh g⁻¹ is obtained for the composite with 40 wt.% Si after 30 cycles. The improvement of the cycle stability of the Si-CeMg₁₂ composite with 40 wt.% Si is mainly attributed to a uniform distribution of active Si nanoparticles embedded in the CeMg₁₂ matrix, which can accommodate the volume expansion of the composite during Li-alloying/dealloying processes. After subsequent cycles, the Si with lattice shrinkage is partially formed due to the recrystallization, which is unfavorable to the Li-alloying/dealloying reaction. Therefore, the degeneration of CeMg₁₂-Si composites during repeated cycling is not only attributed to the Si pulverization led by the volume change, but partially also to the irreversible phase transformation of Si.

Acknowledgement

This work is supported by the 973 Program (2009CB220100), China.

References

[1] B.A. Boukamp, G.C. Lesh, R.A. Huggins, J. Electrochem. Soc. 128 (1981) 725.
 [2] J.J. Niu, J.Y. Lee, Electrochem. Solid-State Lett. 5 (2002) A107.

- [3] J. Yang, B.F. Wang, K. Wang, Y. Liu, J.Y. Xie, Z.S. Wen, *Electrochem. Solid-State Lett.* 6 (2003) A154.
- [4] N. Dimov, S. Kugino, M. Yoshio, *Electrochim. Acta* 48 (2003) 1579.
- [5] S. Park, T. Kim, S.M. Oh, *Electrochem. Solid-State Lett.* 10 (2007) A142.
- [6] S.H. Ng, J.Z. Wang, D. Wexler, S.Y. Chew, H.K. Liu, *J. Phys. Chem. C* 111 (2007) 11131.
- [7] A. Netz, R.A. Huggins, W. Weppner, *J. Power Sources* 119–121 (2003) 95.
- [8] I. Kim, G.E. Blomgren, P.N. Kumta, *J. Power Sources* 130 (2004) 275.
- [9] X.N. Zhang, G.L. Pan, G.R. Li, J.Q. Qu, X.P. Gao, *Solid State Ionics* 178 (2007) 1107.
- [10] H. Dong, R.X. Feng, X.P. Ai, Y.L. Cao, H.X. Yang, *Electrochim. Acta* 49 (2004) 5217.
- [11] J.B. Kim, B.S. Jun, S.M. Lee, *Electrochim. Acta* 50 (2005) 3390.
- [12] Y.L. Kim, H.Y. Lee, S.W. Jang, S.H. Lim, S.J. Lee, H.K. Baik, Y.S. Yoon, S.M. Lee, *Electrochim. Acta* 48 (2003) 2593.
- [13] J.W. Kim, J.H. Ryu, K.T. Lee, S.M. Oh, *J. Power Sources* 147 (2005) 227.
- [14] K. Wang, X.M. He, L. Wang, J.G. Ren, C.Y. Jiang, C.R. Wan, *Solid State Ionics* 178 (2007) 115.
- [15] X.D. Wu, Z.X. Wang, L.Q. Chen, X.J. Huang, *Electrochem. Commun.* 5 (2003) 935.
- [16] X.L. Yang, Z.Y. Wen, X.X. Xu, Z.H. Gu, S.H. Huang, *Electrochem. Solid-State Lett.* 10 (2007) A52.
- [17] M.D. Fleischauer, J.M. Toppole, J.R. Dahna, *Electrochem. Solid-State Lett.* 8 (2005) A137.
- [18] Y.N. Li, B.F. Wang, J. Yang, X.X. Yuan, Z.F. Ma, *J. Power Sources* 153 (2006) 371.
- [19] I. Kim, G.E. Blomgren, P.N. Kumta, *Electrochem. Solid-State Lett.* 6 (2003) A157.
- [20] H. Guo, H.L. Zhao, C.L. Yin, W.H. Qiu, *J. Alloys Compd.* 426 (2006) 277.
- [21] X.N. Zhang, P.X. Huang, G.R. Li, T.Y. Yan, G.L. Pan, X.P. Gao, *Electrochem. Commun.* 9 (2007) 713.
- [22] H. Kim, J. Choi, H.J. Sohn, T. Kang, *J. Electrochem. Soc.* 146 (1999) 4401.
- [23] G.A. Roberts, E.J. Cairns, J.A. Reimer, *J. Power Sources* 110 (2002) 424.
- [24] S.W. Song, K.A. Striebel, R.P. Reade, G.A. Roberts, E.J. Cairns, *J. Electrochem. Soc.* 150 (2003) A121.
- [25] H. Kim, B. Park, H.J. Sohn, T. Kang, *J. Power Sources* 90 (2000) 59.
- [26] C.M. Park, Y.U. Kim, H. Kim, H.J. Sohn, *J. Power Sources* 158 (2006) 1451.
- [27] Y. Wang, Z.W. Lu, Y.L. Wang, T.Y. Yan, J.Q. Qu, X.P. Gao, P.W. Shen, *J. Alloys Compd.* 421 (2006) 236.
- [28] Z.W. Lu, S. Sun, G.R. Li, T.Y. Yan, J.Q. Qu, X.P. Gao, *J. Alloys Compd.* 433 (2007) 269.
- [29] D. Larcher, S. Beattie, M. Morcrette, K. Edstroem, J.C. Jumas, J.M. Tarascon, *J. Mater. Chem.* 17 (2007) 3759.
- [30] L.B. Chen, K. Wang, X.H. Xie, J.Y. Xie, *Electrochem. Solid-State Lett.* 9 (2006) A512.
- [31] H. Li, X.J. Huang, L.Q. Chen, G.W. Zhou, Z. Zhang, D.P. Yu, Y.J. Mo, N. Pei, *Solid State Ionics* 135 (2000) 181.
- [32] P. Limthongkul, Y.I. Jang, N.J. Dudney, Y.M. Chiang, *J. Power Sources* 119–121 (2003) 604.